Arctic sea ice variability during the Instrumental Era

M. Kathleen Brennan[1], Gregory J. Hakim[1], and Edward Blanchard-Wrigglesworth[1]

[1]University of Washington

November 24, 2022

Abstract

Arctic sea-ice extent (SIE) has declined drastically in recent decades, yet its evolution prior to the satellite era is highly uncertain. Studies using SIE observations find little variability prior to the 1970s; however, these reconstructions are based on limited data, especially prior to the 1950s. We use ensemble Kalman filter data assimilation of surface air temperature observations with Last Millennium climate model simulations to create a fully gridded Arctic sea-ice concentration reconstruction from 1850–2018, and investigate the evolution of Arctic SIE during this period. We find a decline of ˜1.25 x 106 km2 during the early 20th-century warming (1910-1940). The 25-year trends during this period are ˜33-38% smaller than the satellite era (1979-2018) but almost twice as large as previous estimates. Additionally we find that variability of SIE on decadal timescales prior to satellite era is ˜40% greater than previously estimated.

Arctic sea ice variability during the Instrumental Era

M. Kathleen Brennan, Gregory J. Hakim, and Edward Blanchard-Wrigglesworth

[1]Department of Atmospheric Sciences, University of Washington

Key Points:

- Data assimilation is a skillful technique for reconstructing Arctic sea-ice extent during the satellite era.
- Reconstructed sea ice shows large decline in total Arctic sea-ice extent during the early 20th-century warming (1910–1940).
- Trends in total Arctic sea-ice extent during the satellite era are ∼33–38 % greater than during the early 20th-century warming.

Corresponding author: M. Kathleen Brennan, `mkb22@uw.edu`

Abstract

Arctic sea-ice extent (SIE) has declined drastically in recent decades, yet its evolution prior to the satellite era is highly uncertain. Studies using SIE observations find little variability prior to the 1970s; however, these reconstructions are based on limited data, especially prior to the 1950s. We use ensemble Kalman filter data assimilation of surface air temperature observations with Last Millennium climate model simulations to create a fully gridded Arctic sea-ice concentration reconstruction from 1850–2018, and investigate the evolution of Arctic SIE during this period. We find a decline of $\sim$1.25 x10^6 km^2 during the early 20th-century warming (1910–1940). The 25-year trends during this period are $\sim$33-38% smaller than the satellite era (1979–2018) but almost twice as large as previous estimates. Additionally we find that variability of SIE on decadal timescales prior to satellite era is $\sim$40% greater than previously estimated.

Plain Language Summary

Arctic sea ice is an important part of the climate system, serving as the interface between the ocean–atmosphere system. Arctic sea ice has undergone rapid declines in recent decades, prompting the question of whether there have been changes of similar magnitude in the past. To answer such questions, a long record of sea ice is necessary, but spatially and temporally complete satellite observations are only available starting in 1979. Previous studies combining sea ice observations from various sources during the Instrumental Era (1850–2014) found little variability in sea-ice extent prior to the satellite era, but data availability is limited prior to the 1950s. Here we create an independent estimate of Arctic sea ice from 1850–2018 using a data assimilation approach that blends more abundant temperature observations with data from climate models. Our results show substantial loss of sea ice between 1910–1940, with a rate that is about $\sim$33-38% less than what has been observed in satellite observations. These results reinforce previous findings that the current trend is unprecedented in duration since 1850, but also that sea-ice variability prior to 1979 is $\sim$40% larger than previously estimated.

1 Introduction

Arctic sea ice is one of the most rapidly changing components of the climate system, affecting surface albedo and modulating ocean–atmosphere interaction through surface fluxes. Large declines in sea ice can impact local ecosystems, human communities, and the global climate system (Meier et al., 2014). Documenting and understanding decadal–centennial variability in sea ice is limited by the availability of high-quality observations, which are only spatially and temporally complete during the satellite era (1978–present) (Fetterer et al., 2017). Furthermore, given the presence of strong radiative forcing during this period, it is difficult to partition the relative role of natural variability (e.g. Ding et al. (2017); England et al. (2019)) and radiative forcing (Notz & Marotzke, 2012) on the rapid Arctic sea ice declines observed in the satellite record. In order to estimate the natural variability of sea ice, a longer record is needed. Here we introduce a novel method to reconstruct sea ice cover from 1850–present, using data assimilation (DA), numerical model data, and observations of surface air temperature (SAT).

The longest Arctic sea-ice extent (SIE) observation-based reconstruction combines various sea ice observation types, ranging from satellite data to shipping records, to extend Arctic sea ice records back to 1850 (Walsh et al., 2017). The Walsh et al. (2017) reconstruction shows little SIE variability before 1970, particularly on decadal to multidecadal timescales. However, the fidelity of this dataset is limited by gaps in observation availability, particularly before 1953 and during winter months (see below and Supporting Information Figure S1).

Although direct observations of sea ice are limited in space and time, instrumental observations of SAT are much more abundant. Polar, hemispheric and global mean SAT, both in observations and climate models, are known to be tightly coupled to sea ice variability on annual and longer timescales (e.g. Gregory et al. (2002); Armour et al. (2011); Mahlstein and Knutti (2012); Olonscheck et al. (2019)). Observations show that global-mean SAT was relatively stable between 1850–1900 (Morice et al., 2012), which may explain low decadal sea ice variability in the Walsh et al. (2017) record. However, during the early 20th century (1900–1940), an anomalous warming event is well documented across Northern Hemisphere high latitudes (e.g. Hegerl et al. (2018)). The magnitude of this early 20th century warming (ETCW) was largest during winter months (Semenov, 2007; Overland et al., 2004) and similar in spatial structure to that observed in the late 20th century.

Interestingly, the Walsh et al. (2017) record of Arctic SIE shows much less decline during the ETCW than during the satellite record, with one period of decline of $\sim$0.5 x 10^6 km^2 between 1920-1945 followed by a recovery of $\sim$0.5 x 10^6 km^2 between 1945–1950 (see below). The peak loss in Walsh et al. (2017) also lags the period of largest ETCW temperature anomalies seen in observations, which together with the modest decline in SIE suggests a weak relationship between temperature and sea ice during the ETCW. In this paper we investigate the relationship between temperature and sea ice during the Instrumental Era using satellite observations, reanalysis, and the Walsh et al. (2017) reconstruction. Then we use a DA framework to construct a new independent Arctic sea ice reconstruction using more abundant SAT observations. We then explore the decline of sea ice during the ETCW, and compare the ETCW decline to that observed and reconstructed in the satellite era.

2 Temperature and sea ice in the Instrumental Era

We begin by analyzing the relationship between Arctic SAT derived from the HadCRUT4.6.0.0 dataset (HadCRUT, Morice et al. (2012)) and SIE from Walsh et al. (2017). We partition the analysis in two ways: by season (April–August and September–March) and by time period (pre- and post-1953 for Walsh et al. (2017), plus the satellite era (1979–2017)), in order to investigate the effect of observation availability on the Walsh et al. (2017) record. We find that the relationship between SAT and SIE from the Walsh et al. (2017) and satellite observations generally agree from 1953–present, but differ greatly before 1953 (Figure 1).

Figure 1 shows that the relationship between SAT and SIE is linear in the satellite record in both seasons, with R^2=0.76 (September–March) and 0.85 (April–August). The Walsh et al. (2017) record also shows a linear relationship for both seasons between 1953–2013, with a similar slope during winter (Figure 1b) and a slightly steeper slope during summer (Figure 1a), both not statistically different from the slope determined with satellite observations at the 95% confidence level. In contrast, the earlier part of the Walsh et al. (2017) record, between 1850–1952, exhibits a much lower SIE–SAT sensitivity in summer relative to the satellite era (Figure 1a) and almost no SIE–SAT sensitivity in winter (Figure 1b). Since SAT is a primary driver of sea ice variability (Olonscheck et al., 2019), the inconsistent relationship between these two time periods in the Walsh et al. (2017) record suggests either a strong nonlinearity in this relationship during the ETCW, or that the reconstruction underestimates SIE-SAT sensitivity.

There are at least two possible hypothesis for the reduced sensitivity of SIE-SAT in Walsh et al. (2017) before 1953. Firstly, the sensitivity of sea ice to temperature may be mean-state dependent, such that in colder, thicker, sea-ice regimes (which may have existed in the Arctic during the late 19th and early 20th century) sea ice may be less sensitive to changes in temperature. However, model simulations of sea-ice sensitivity to temperature for different mean states (Armour et al., 2011; Mahlstein & Knutti, 2012) do

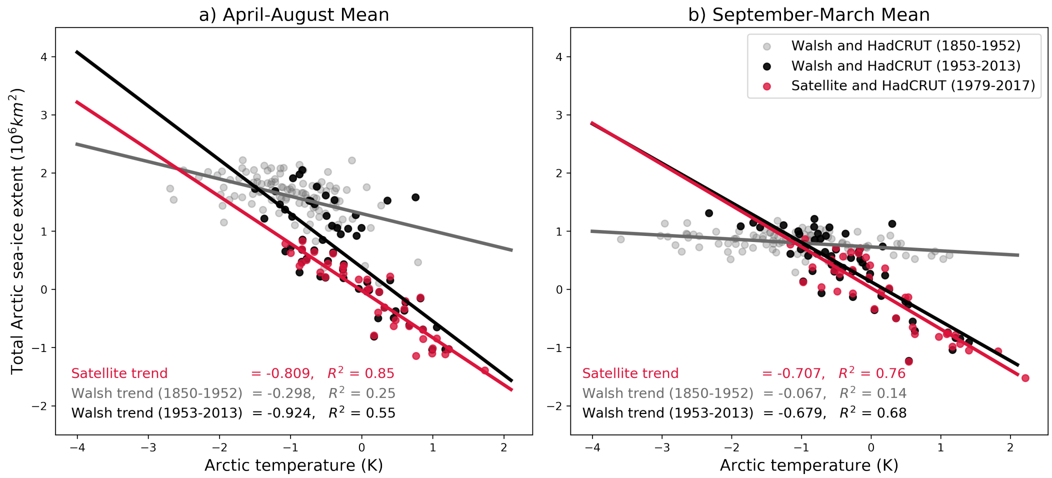

Figure 1. Arctic SAT (averaged north of $65°N$, derived from HadCRUT) and total SIE in both the satellite data between 1979-2017 (in red) and the Walsh et al. (2017) data set between 1850 to 1952 (in gray) and 1953 to 2013 (in black). Anomalies are relative to 1979-2013.

not support this hypothesis. A second hypothesis is that the reduced sensitivity of sea ice to temperature may simply be due to the fact that there are significantly fewer observations available to the Walsh et al. (2017) analysis prior to 1953 (as illustrated in Supporting Information Figure S1).

The fidelity of sea-ice reconstructions has broader implications, as they are used for boundary conditions in reanalysis products. The widely-used sea surface temperature and sea ice concentration HadISST2 product (Titchner & Rayner, 2014) incorporates an earlier version of the Walsh et al. (2017) sea-ice reconstruction (Walsh & Chapman, 2001), which is based largely on climatology for the first half of the 20th century. Atmospheric reanalysis during the 20th century such as ERA-20C (Poli et al., 2016) commonly use HadISST2 as a boundary condition. Figure 2 shows temperature trends in ERA-20C and the station-based HadCRUT (which uses no infill or interpolation). While HadCRUT shows the large magnitudes and spatial extent of SAT trends during the ETCW, in some locations comparable to the that during the recent satellite-era warming, ERA-20C shows minimal trends across the Arctic. The NOAA/CIRES 20th Century reanalysis (Compo et al., 2011) shows even larger biases than ERA-20C (see Supporting Information Figure S2).

We postulate that these atmospheric reanalysis biases in simulating the ETCW are strongly influenced by the small inter-annual sea-ice variability in Walsh and Chapman (2001) that serve as boundary conditions. This hypothesis is consistent with Semenov and Latif (2012), who find that the ETCW cannot be simulated with an atmospheric model forced with HadISST1.1 (Rayner, 2003) boundary conditions, which show little sea-ice variability prior to 1950. Thus improving sea-ice reconstructions has broad implications, especially for studying high latitude climate variability.

To this end, we exploit the linear relationship between SAT and Arctic SIE evident in Figure 1 and in the literature (Mahlstein & Knutti, 2012) to reconstruct sea ice using a DA approach. Other approaches have exploited this relationship to reconstruct sea ice in the 20th century using linear regression models. For example, Connolly et al. (2017) use pre-satellite temperature trends to re-calibrate sea-ice data sources from three regions in the Arctic and find that sea ice retreated after the 1910s and advanced after the mid 1940s, though the magnitude of these changes are small relative to the satellite

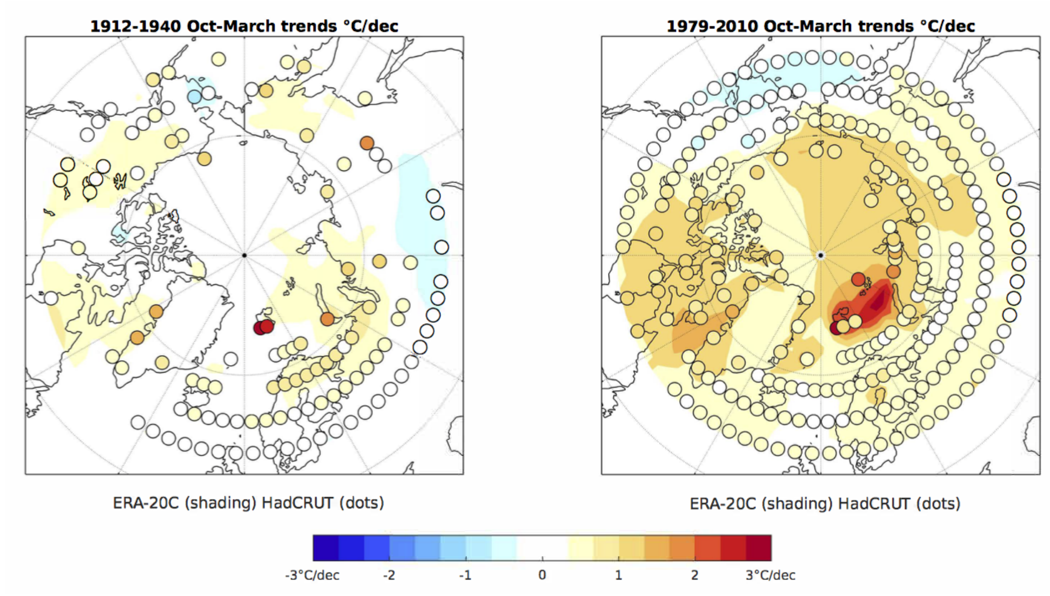

Figure 2. Temperature trends from ERA-20C are shown in shading and that from HadCRUT overlaid as shaded dots for both the early 20th century (1912–1940, left) and satellite era (1979–2010, right).

era. Alekseev et al. (2016) use the relationship between summer SAT and SIE to reconstruct total Arctic SIE with a linear regression model, finding a decline of total Arctic SIE of $\sim$2 x 10^6 km^2 between 1900–1940 followed by a recovery that peaked around 1970. The main benefit of the DA approach described here is the use of high quality 2 mair temperature observations with a robust framework for uncertainty quantification (see Section 3). Moreover, the results provide fully-gridded, spatially consistent climate fields that can be used as boundary conditions for models and to probe the dynamics associated with sea-ice variability.

3 A new sea-ice reconstruction using data assimilation

3.1 Data Assimilation approach

DA aims to optimally combine spatial data with noisy and sparse observations, resulting in a better estimate of climate fields. Generally, DA updates a prior estimate, an initial 'best guess', of the climate state with new information from observations. DA allows point-wise observations of temperature to influence broader spatial regions of other climate variables, like sea ice, based on the covariance relationships derived from the prior. The prior estimate and observations are weighted based on their relative uncertainty, yielding continuous fields.

To reconstruct Arctic sea ice we use an offline (Oke et al., 2002) ensemble Kalman filter approach to combine Last Millennium climate model simulations (Schmidt et al., 2011; Taylor et al., 2012) with temperature observations. The prior, $\mathbf{x}^b$, is an ensemble of 200 random years drawn from these Last Millennium simulations (more details are provided in Section 3.2). The update to this prior estimate uses annually averaged temperature observations, $\mathbf{y}$, weighted as $\mathbf{y} - \mathbf{H}\mathbf{x}^b$ (the 'innovation'),

$$\mathbf{x}^a = \mathbf{x}^b + \mathbf{K}(\mathbf{y} - \mathbf{H}\mathbf{x}^b). \quad (1)$$

The innovation weight that results in the analysis, $\mathbf{x^a}$, is given by the Kalman gain,

$$\mathbf{K} = \mathbf{B}\mathbf{H}^{\mathrm{T}}(\mathbf{H}\mathbf{B}\mathbf{H}^{\mathrm{T}} + \mathbf{R})^{-1}, \tag{2}$$

where $\mathbf{B}$ is the error covariance matrix of the prior, $\mathbf{R}$ is the error covariance matrix of the observations, and T is the transpose operator. Matrix $\mathbf{H}$ maps the prior to the observations by selecting grid-point data in the prior nearest to the observations. The Kalman gain spreads the new information from temperature observations both spatially and to other climate variables, weighted by the relative uncertainty of each. We sample temperature observations from instrumental datasets every 10° latitude and longitude, chosen to ensure the observation errors are uncorrelated and therefore $\mathbf{R}$ is diagonal. This assumption allows us to use serial observation processing, which assimilates observations one at a time, simplifying implementation of spatial covariance localization as described below.

To solve (1), we employ a square-root ensemble Kalman filter (Whitaker & Hamill, 2002), which updates the ensemble mean and the perturbations from the ensemble mean separately. The Kalman gain used in the update equation for the ensemble perturbations ($\tilde{\mathbf{K}}$) is adjusted by a constant α to yield the correct posterior covariance matrix. Therefore, $\tilde{\mathbf{K}} = \alpha\mathbf{K}$, where, for a single observation, i,

$$\alpha = \left(1 + \sqrt{\frac{\mathbf{R}_{ii}}{\mathbf{H}\mathbf{B}\mathbf{H}^{T}{}_{ii} + \mathbf{R}_{ii}}}\right)^{-1}, \tag{3}$$

where ii denotes the matrix diagonal entry in the ith row and column.

As is standard practice in ensemble DA, we reduce the effect of spurious long-distance covariances using covariance localization (e.g. Hamill et al. (2001)), applying the Gaspari-Cohn fifth order polynomial function (Gaspari & Cohn, 1999) with a localization radius (the distance from observations set to zero influence) of 15,000 km.

Kalman filter methods rely on the covariance in the prior ensemble between temperature and the variables of interest (here, sea ice concentration, SIC). Climate models tend to underestimate the sensitivity of Arctic sea-ice loss to temperature (Rosenblum & Eisenman, 2017; Winton, 2011; Stroeve et al., 2007). To address this low-sensitivity bias, we inflate the sea-ice perturbations from the prior ensemble-means for the simulations used here, MPI and CCSM4 Last Millennium simulations (see Section 3.2), by a factor of 1.8 and 2.6, respectively. The inflation factors are determined empirically by goodness of fit to the observed sea-ice trend during the satellite era. Sensitivity of the results to the localization radius and inflation factor is explored below and in the Supporting Information (see figures S4 and S5).

Since the Kalman filter method assumes Gaussian distributions, and SIC has a range of 0–100%, unphysical values of $\mathbf{x^a}$ outside this range may occur. Therefore, SIC values outside the lower and upper end of this range are adjusted to 0% and 100%, respectively.

3.2 Data Sources

A 200-member prior ensemble of both SAT and SIC fields are randomly drawn from fully forced Last Millennium model simulations spanning the years 850–1849 CE (Schmidt et al., 2011; Taylor et al., 2012) (tests with a 1000-member prior ensemble revealed small differences in Arctic SIE reconstructions, $R^2 > 0.97$, from the less computationally expensive case with a 200 member prior ensemble). Results using the Community Climate System Model version 4 (CCSM4, Last Millennium simulation (Landrum et al., 2013)) and Max Planck Institute for Meteorology (MPI-ESM-P, Last Millennium simulation (Taylor et al., 2012)) models are used to determine the sensitivity of the sea-ice reconstructions to climate-model prior, and thus the sensitivity of the results to model physics and sea-ice–temperature covariance structure. All model output is regridded to a $\sim 2°\text{x}2°$ grid.

Sensitivity to the choice of instrumental temperature record is tested using three different products: HadCRUT, Berkeley Earth (BE, (Rohde et al., 2013)), and NASA Goddard Institute for Space Studies (GISTEMP, (Hansen et al., 2010)). An estimate of the uncertainty in these observations is required when using an ensemble Kalman filter approach (i.e., $\mathbf{R}$ in Equations 2 and 3), and HadCRUT is the only product that provides uncertainty estimates. Various ways of calculating $\mathbf{R}$ were tested, (see Supporting Information), but in order to use all three products, and for simplicity, we use an uncertainty estimate of 0.4 K^2, which is the area-weighted mean error variance provided by HadCRUT.

4 Arctic sea-ice reconstructions

We first reconstruct annual Arctic SIC for 1850–2018 by assimilating HadCRUT SAT with a prior ensemble drawn from the MPI Last Millennium simulation. Figure 3 shows annual Arctic SIE (total area with SIC greater than or equal to 15%) derived from the gridded SIC reconstructions. The timeseries is the mean of 5 independent iterations that each use a different 200 member prior ensemble, in order to take into account the uncertainty due to sampling error. Our reconstruction compares well with satellite observations (Figure 3) with R^2 value of 0.89, detrended R^2 value of 0.43, and coefficient of efficiency (see Supporting Information Equation 1) of 0.89 between 1979–2017. The trend during this period is well captured in the reconstructions with a value of -0.052 ± 0.012 x 10^6 km^2/year compared to -0.055 x 10^6 km^2/year in satellite observations. Inter-annual variability is overestimated, with a detrended standard deviation of 0.21 x 10^6 km^2 in the satellite observations and 0.28 x 10^6 km^2 in the reconstruction during 1979–2017.

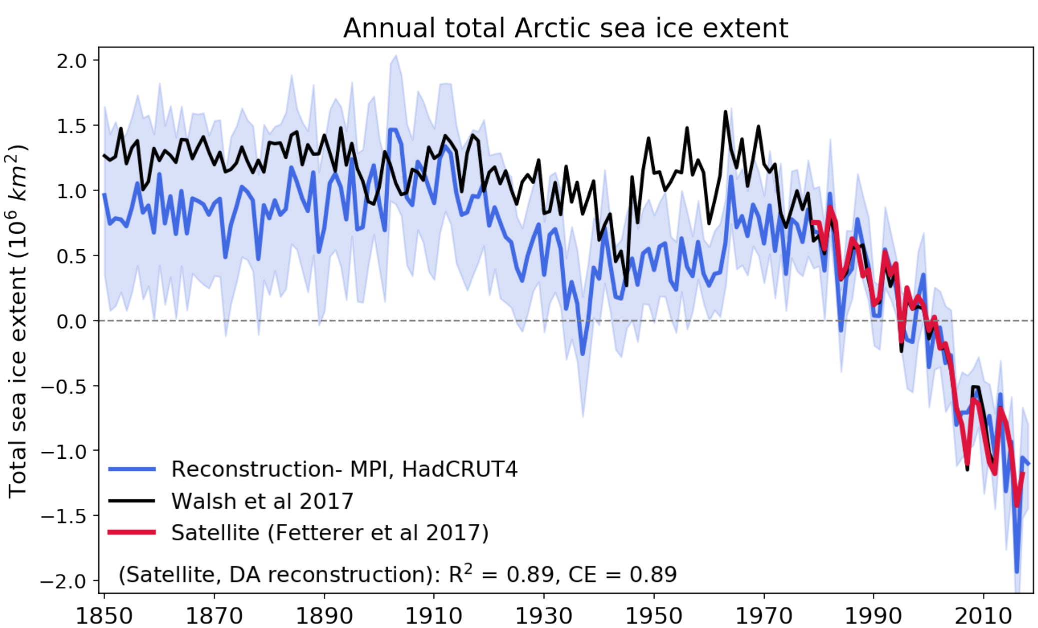

Figure 3. Reconstructed Arctic SIE from DA (blue), Walsh et al. (2017) (black), and satellite observations (red). For our reconstructions annually averaged HadCRUT temperature data was assimilated with a prior ensemble drawn from the MPI Last Millennium simulation. Anomalies are centered about 1979–2013.

The most notable feature of our reconstruction before the satellite era is the SIE decline during the ETCW, with a total loss of about 1.25 x 10^6 km^2 between 1910–1940 compared to $\sim$2.0 x 10^6 km^2 lost between 1979–2017 in satellite observations. Between 1930–1950, our reconstruction also shows $\sim$0.5 x 10^6 km^2 less SIE than in the Walsh et al. (2017) SIE record (see Figure 3), and the ETCW minimum occurs approximately eight years earlier than in Walsh et al. (2017). Between 1850–1900 our reconstruction shows a slow increase in SIE, reaching a maximum just after 1900, as opposed to the Walsh et al. (2017) record which shows maximum SIE in the 1960s. Overall, prior to the satellite era our reconstruction shows greater decadal variability compared to the Walsh et al. (2017) record, which has relatively constant Arctic SIE between 1850–1970. Prior to the satellite era (1850–1979) our reconstruction has a time-series standard deviation of 310,000 km^2 whereas the Walsh et al. (2017) record has standard deviation of 220,000 km^2. Though our reconstructions are annually resolved, they generally agree with the summer reconstructions of Arctic SIE in Alekseev et al. (2016).

4.1 Trends and variability

Next, we investigate the magnitude and significance of Arctic SIE trends during the ETCW relative to the satellite era. In our reconstructions, the SIE decline in the ETCW is shorter lived ($\sim$25–30 years) than that in the satellite era ($\sim$40 years), thus we investigate the distribution of 25-year trends for both the satellite era and ETCW.

Figure 4 shows the distribution of trends calculated for each ensemble member (from reconstructions using both MPI and CCSM4 model priors) for all possible 25-year segments during the satellite era (1979–2017) and the ETCW (1910–1940). The distribution of all 25-year trends between 1979–2017 for both Walsh et al. (2017) and satellite observations are also shown as boxplots below the distributions. For the Walsh et al. (2017) record, ETCW trends were calculated between 1918–1948 and are also shown as a boxplot (we use a later window for a fair comparison since the minimum SIE occurred 8 years later in Walsh et al. (2017)). The median 25-year trend found in the Walsh et al. (2017) record during the ETCW of -0.18 x 10^6 km^2/year falls at the 98th and 99th percentiles of the MPI and CCSM4 model prior reconstructions, respectively. We note that our reconstructions slightly underestimate the mean 25-year trend in the satellite era. However, when comparing these two time periods in our reconstructions, the satellite era trends are $\sim$33–38% greater than the ETCW trends.

4.2 Sensitivity of results

Our reconstruction of SIE depends on the gridded temperature product assimilated (and associated errors), on the climate model prior, and on sample-error mediation in the DA (localization length scale and ensemble variance inflation factor). A range of choices for these aspects have been tested, with details provided in the Supporting Information. Overall we find that the choice of observational dataset and model prior make little difference to pan-Arctic indices (see Figure S3 in Supporting Information), but that variance inflation and spatial localization have a larger affect.

With an offline DA approach, all temporal variability in the reconstruction comes from the observations. Thus, increasing the localization radius and the ensemble variance inflation of sea ice relative to temperature, both increase the influence of temperature observations, which is realized as larger temporal variability (Figure S4 and S5 in Supporting Information). The results indicate a trade-off between capturing decadal variability versus inter-annual variability. For the MPI prior assimilated with HadCRUT temperature, a localization length scale of 15,000 km leads to the best reconstructed trend for nearly all inflation factors, so we chose to use this localization length scale. Given a localization length scale of 15,000 km, the skill metrics are best for an inflation factor of 1.8. For a prior drawn from the CCSM4 Last Millennium simulation and HadCRUT

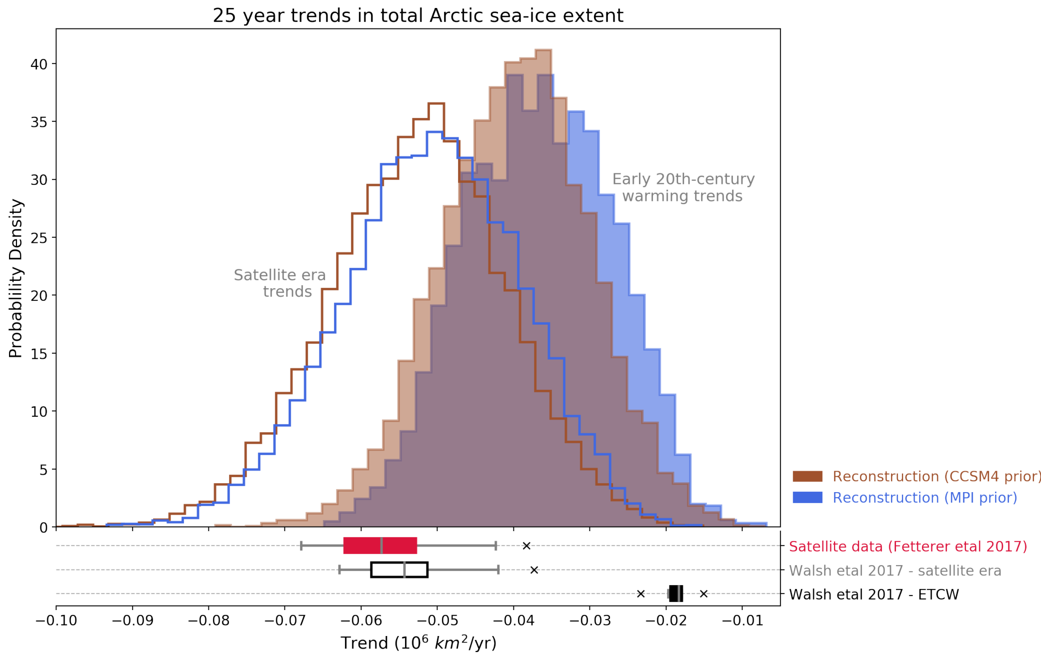

Figure 4. The distribution of all possible 25-year trends in Arctic SIE during the satellite era (1979–2017) and ETCW (1910–1940) for 5 prior iterations, each containing 200 ensemble members. The probability density functions show reconstructed SIE trends using MPI as the model prior (blue) and CCSM4 (brown). Below the histograms, the spread of trends calculated in the Walsh et al. (2017) record (black) and satellite observations (red) are displayed as box plots. The ETCW for the Walsh et al. (2017) record was calculated between 1918–1948.

observations, the same localization length scale of 15,000 km was used and an inflation factor of 2.6 gave the best skill scores. Overall, these experiments show that a range of values of localization and ensemble inflation result in skillful reconstructions relative to satellite observations, and similar reconstructions of sea ice for earlier time periods.

5 Conclusions

The relationship between SIE and SAT is linear during the satellite era in observations, but we find that this relationship is much weaker or even absent in the Walsh et al. (2017) record of SIE prior to the 1950s. This lower sensitivity of SIE to SAT in the Walsh et al. (2017) record is plausibly due to a lack of high quality sea-ice observations, especially during fall and winter and prior to 1953. We have also found that 20th century atmospheric reanalysis underestimate the magnitude of the ETCW (1910-1940) in the Arctic. Since previous versions of the Walsh et al. (2017) dataset are used as boundary conditions for 20th-century atmospheric reanalysis, we speculate that the low variability of SIE in Walsh et al. (2017) could be a reason atmospheric reanalysis do not fully capture the ETCW, but leave exploration of this hypothesis to future work.

We exploit the relationship between SAT and SIC using an ensemble Kalman filter data assimilation approach to produce a new sea-ice reconstruction. This method optimally combines temperature observations and model data from Last Millennium simulations to yield skillful Arctic sea-ice reconstructions with annual resolution. Validation against satellite observations yields an R^2-value of 0.89 and coefficient of efficiency of 0.89. Prior to the satellite era, our reconstructions show Arctic SIE loss of ~1.25 x

10^6 km^2 during the ETCW, which is greater than the ETCW loss of ∼0.75–1.0 x 10^6 km^2 estimated in Walsh et al. (2017), yet smaller than the SIE loss during the satellite era of ∼2.0 x 10^6 km^2. The reconstructed 25-year trends of SIE indicate that the rate of sea-ice loss during the ETCW was about ∼33–38% smaller than the 25-year trends during the satellite era.

Overall, these reconstructions show more inter-annual variability in SIE than in Walsh et al. (2017) during the Instrumental Era with standard deviation ∼40% (∼90,000 km^2) greater between 1850–1979, a significant part due to the ETCW. The ETCW has been ascribed to a combination of anthropogenic forcing and strong natural variability (Fyfe et al., 2013; Delworth, 2000; Wood & Overland, 2009; Beitsch et al., 2014). Here we find that during the satellite era, Arctic sea-ice loss was larger and longer lasting than during the ETCW, which implies that the current declines likely necessitate external anthropogenic forcing, as previous results have shown (Ding et al., 2017; Kay et al., 2011; Notz & Marotzke, 2012). Future work will extend this approach to reconstructing seasonal variability and sea-ice thickness to further our understanding of sea ice during the Instrumental era.

Acknowledgments

The data for these reconstructions will be uploaded to Zenodo upon acceptance. The authors thank Cecilia Bitz and David Battisti for comments and ideas leading to this project. MKB thanks Luke Parsons for insights into comparing trends and for testing localization and inflation; Robert Tardif for contribution to development of the DA code; Andre Perkins for software debugging help; Jessica Badgeley for productive discussions and support; and Robert Brennan for editing help. MKB was supported by the NSF GRFP program. GH was supported by NSF award AGS-1602223 and NOAA award NA18OAR4310422. EBW was supported by NOAA MAPP grant NA18OAR4310274.

References

Alekseev, G., Glok, N., & Smirnov, A. (2016). On assessment of the relationship between changes of sea ice extent and climate in the Arctic. *International Journal of Climatology*, *36*(9), 3407–3412. doi: 10.1002/joc.4550

Armour, K. C., Eisenman, I., Blanchard-Wrigglesworth, E., McCusker, K. E., & Bitz, C. M. (2011, aug). The reversibility of sea ice loss in a state-of-the-art climate model. *Geophysical Research Letters*, *38*(16), n/a–n/a. doi: 10.1029/2011GL048739

Beitsch, A., Jungclaus, J. H., & Zanchettin, D. (2014, oct). Patterns of decadal-scale Arctic warming events in simulated climate. *Climate Dynamics*, *43*(7-8), 1773–1789. doi: 10.1007/s00382-013-2004-5

Compo, G. P., Whitaker, J. S., Sardeshmukh, P. D., Matsui, N., Allan, R. J., Yin, X., ... Worley, S. J. (2011, jan). The Twentieth Century Reanalysis Project. *Quarterly Journal of the Royal Meteorological Society*, *137*(654), 1–28. doi: 10.1002/qj.776

Connolly, R., Connolly, M., & Soon, W. (2017). Re-calibration of Arctic sea ice extent datasets using Arctic surface air temperature records. *Hydrological Sciences Journal*, *62*(8), 1317–1340. doi: 10.1080/02626667.2017.1324974

Delworth, T. L. (2000, mar). Simulation of Early 20th Century Global Warming. *Science*, *287*(5461), 2246–2250. doi: 10.1126/science.287.5461.2246

Ding, Q., Schweiger, A., L'Heureux, M., Battisti, D. S., Po-Chedley, S., Johnson, N. C., ... Steig, E. J. (2017, apr). Influence of high-latitude atmospheric circulation changes on summertime Arctic sea ice. *Nature Climate Change*, *7*(4), 289–295. doi: 10.1038/nclimate3241

England, M., Jahn, A., & Polvani, L. (2019). Nonuniform contribution of internal variability to recent Arctic sea ice loss. *Journal of Climate*, *32*(13), 4039–4053. doi: 10.1175/JCLI-D-18-0864.1

Fetterer, F., Knowles, K., Meier, W. N., Savoie, M., & Windnagel, A. K. (2017). Sea Ice Index, Version 3. *NSIDC: National Snow and Ice Data Center, Boulder, Colorado USA*. doi: 10.7265/N5K072F8

Fyfe, J. C., von Salzen, K., Gillett, N. P., Arora, V. K., Flato, G. M., & McConnell, J. R. (2013, dec). One hundred years of Arctic surface temperature variation due to anthropogenic influence. *Scientific Reports*, *3*(1), 2645. doi: 10.1038/srep02645

Gaspari, G., & Cohn, S. E. (1999, jan). Construction of correlation functions in two and three dimensions. *Quarterly Journal of the Royal Meteorological Society*, *125*(554), 723–757. doi: 10.1256/smsqj.55416

Gregory, J. M., Stott, P. A., Cresswell, D. J., Rayner, N. A., Gordon, C., & Sexton, D. M. H. (2002, dec). Recent and future changes in Arctic sea ice simulated by the HadCM3 AOGCM. *Geophysical Research Letters*, *29*(24), 28–1–28–4. doi: 10.1029/2001GL014575

Hamill, T. M., Whitaker, J. S., & Snyder, C. (2001, nov). Distance-Dependent Filtering of Background Error Covariance Estimates in an Ensemble Kalman Filter. *Monthly Weather Review*, *129*(11), 2776–2790. doi: 10.1175/1520-0493(2001)129⟨2776:DDFOBE⟩2.0.CO;2

Hansen, J., Ruedy, R., Sato, M., & Lo, K. (2010, dec). GLOBAL SURFACE TEMPERATURE CHANGE. *Reviews of Geophysics*, *48*(4), RG4004. doi: 10.1029/2010RG000345

Hegerl, G. C., Brönnimann, S., Schurer, A., & Cowan, T. (2018, jul). The early 20th century warming: Anomalies, causes, and consequences. *Wiley Interdisciplinary Reviews: Climate Change*, *9*(4), e522. doi: 10.1002/wcc.522

Kay, J. E., Holland, M. M., & Jahn, A. (2011, aug). Inter-annual to multi-decadal Arctic sea ice extent trends in a warming world. *Geophysical Research Letters*, *38*(15), 2–7. doi: 10.1029/2011GL048008

Landrum, L., Otto-Bliesner, B. L., Wahl, E. R., Conley, A., Lawrence, P. J., Rosenbloom, N., & Teng, H. (2013, feb). Last Millennium Climate and Its Variability in CCSM4. *Journal of Climate*, *26*(4), 1085–1111. doi: 10.1175/JCLI-D-11-00326.1

Mahlstein, I., & Knutti, R. (2012, mar). September Arctic sea ice predicted to disappear near 2C global warming above present. *Journal of Geophysical Research: Atmospheres*, *117*(D6), n/a–n/a. doi: 10.1029/2011JD016709

Meier, W. N., Hovelsrud, G. K., van Oort, B. E., Key, J. R., Kovacs, K. M., Michel, C., … Reist, J. D. (2014, sep). Arctic sea ice in transformation: A review of recent observed changes and impacts on biology and human activity. *Reviews of Geophysics*, *52*(3), 185–217. doi: 10.1002/2013RG000431

Morice, C. P., Kennedy, J. J., Rayner, N. A., & Jones, P. D. (2012, apr). Quantifying uncertainties in global and regional temperature change using an ensemble of observational estimates: The HadCRUT4 data set. *Journal of Geophysical Research: Atmospheres*, *117*(D8), n/a–n/a. doi: 10.1029/2011JD017187

Notz, D., & Marotzke, J. (2012, apr). Observations reveal external driver for Arctic sea-ice retreat. *Geophysical Research Letters*, *39*(8), n/a–n/a. doi: 10.1029/2012GL051094

Oke, P. R., Allen, J., Miller, R. N., Egbert, G. D., & Kosro, P. M. (2002). Assimilation of surface velocity data into a primitive equation coastal ocean model. *Journal of Geophysical Research*, *107*(C9), 3122. doi: 10.1029/2000JC000511

Olonscheck, D., Mauritsen, T., & Notz, D. (2019, jun). Arctic sea-ice variability is primarily driven by atmospheric temperature fluctuations. *Nature Geoscience*, *12*(6), 430–434. doi: 10.1038/s41561-019-0363-1

Overland, J. E., Spillane, M. C., Percival, D. B., Wang, M., & Mofjeld, H. O. (2004, sep). Seasonal and Regional Variation of Pan-Arctic Surface Air Temperature over the Instrumental Record*. *Journal of Climate*, *17*(17), 3263–3282. doi: 10.1175/1520-0442(2004)017⟨3263:SARVOP⟩2.0.CO;2

Poli, P., Hersbach, H., Dee, D. P., Berrisford, P., Simmons, A. J., Vitart, F., ... Fisher, M. (2016, jun). ERA-20C: An Atmospheric Reanalysis of the Twentieth Century. *Journal of Climate*, *29*(11), 4083–4097. doi: 10.1175/JCLI-D-15-0556.1

Rayner, N. A. (2003). Global analyses of sea surface temperature, sea ice, and night marine air temperature since the late nineteenth century. *Journal of Geophysical Research*, *108*(D14), 4407. doi: 10.1029/2002JD002670

Rohde, R., Muller, R., Jacobsen, R., Perlmutter, S., & Mosher, S. (2013). Berkeley Earth Temperature Averaging Process. *Geoinformatics & Geostatistics: An Overview*, *01*(02). doi: 10.4172/2327-4581.1000103

Rosenblum, E., & Eisenman, I. (2017, aug). Sea Ice Trends in Climate Models Only Accurate in Runs with Biased Global Warming. *Journal of Climate*, *30*(16), 6265–6278. doi: 10.1175/JCLI-D-16-0455.1

Schmidt, G. A., Jungclaus, J. H., Ammann, C. M., Bard, E., Braconnot, P., Crowley, T. J., ... Vieira, L. E. A. (2011, jan). Climate forcing reconstructions for use in PMIP simulations of the last millennium (v1.0). *Geoscientific Model Development*, *4*(1), 33–45. doi: 10.5194/gmd-4-33-2011

Semenov, V. A. (2007). Structure of temperature variability in the high latitudes of the Northern Hemisphere. *Izvestiya - Atmospheric and Ocean Physics*, *43*(6), 687–695. doi: 10.1134/S0001433807060023

Semenov, V. A., & Latif, M. (2012, nov). The early twentieth century warming and winter Arctic sea ice. *The Cryosphere*, *6*(6), 1231–1237. doi: 10.5194/tc-6-1231-2012

Stroeve, J., Holland, M. M., Meier, W., Scambos, T., & Serreze, M. (2007, may). Arctic sea ice decline: Faster than forecast. *Geophysical Research Letters*, *34*(9), 1–5. doi: 10.1029/2007GL029703

Taylor, K. E., Stouffer, R. J., & Meehl, G. A. (2012). An Overview of CMIP5 and the Experiment Design. *American Meteorological Society*.

Titchner, H. A., & Rayner, N. A. (2014, mar). The Met Office Hadley Centre sea ice and sea surface temperature data set, version 2: 1. Sea ice concentrations. *Journal of Geophysical Research: Atmospheres*, *119*(6), 2864–2889. doi: 10.1002/2013JD020316

Walsh, J. E., & Chapman, W. L. (2001). 20Th-Century Sea-Ice Variations From Observational Data. *Annals of Glaciology*, *33*(1979), 444–448.

Walsh, J. E., Fetterer, F., Scott Stewart, J., & Chapman, W. L. (2017, jan). A database for depicting Arctic sea ice variations back to 1850. *Geographical Review*, *107*(1), 89–107. doi: 10.1111/j.1931-0846.2016.12195.x

Whitaker, J. S., & Hamill, T. M. (2002). Ensemble Data Assimilation without Perturbed Observations. *Monthly Weather Review*, *130*(7), 1913–1924. doi: 10.1175/1520-0493(2002)130⟨1913:edawpo⟩2.0.co;2

Winton, M. (2011). Do climate models underestimate the sensitivity of Northern Hemisphere sea ice cover? *Journal of Climate*, *24*(15), 3924–3934. doi: 10.1175/2011JCLI4146.1

Wood, K. R., & Overland, J. E. (2009). Early 20 th century Arctic warming in retrospect. *International Journal of Climatology*, *30*(9), n/a–n/a. doi: 10.1002/joc.1973

Figure 1.

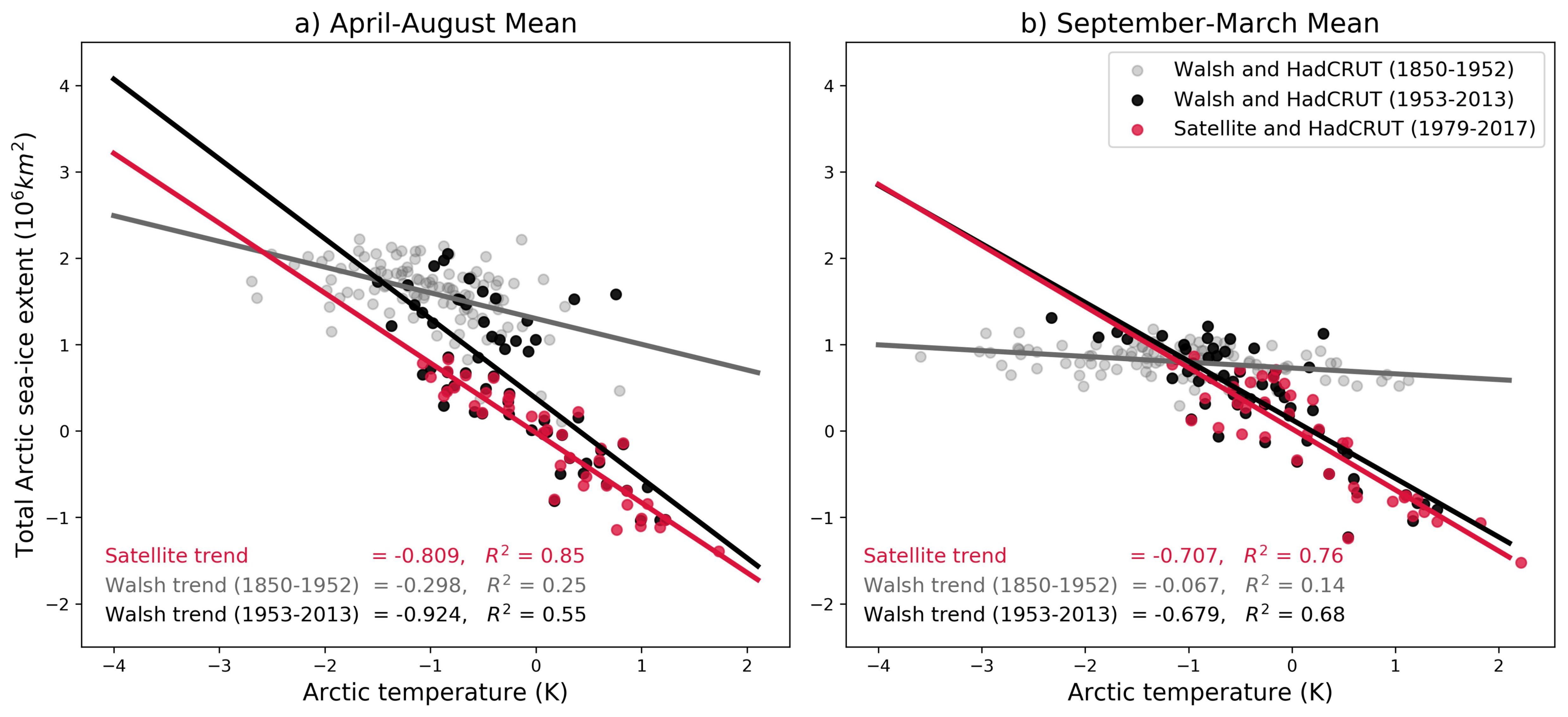

a) April-August Mean
b) September-March Mean
Walsh and HadCRUT (1850-1952)
Walsh and HadCRUT (1953-2013)
Satellite and HadCRUT (1979-2017)
Total Arctic sea-ice extent ($10^6 km^2$)
Arctic temperature (K)
Satellite trend = -0.809, R^2 = 0.85
Walsh trend (1850-1952) = -0.298, R^2 = 0.25
Walsh trend (1953-2013) = -0.924, R^2 = 0.55
Satellite trend = -0.707, R^2 = 0.76
Walsh trend (1850-1952) = -0.067, R^2 = 0.14
Walsh trend (1953-2013) = -0.679, R^2 = 0.68

Figure 2.

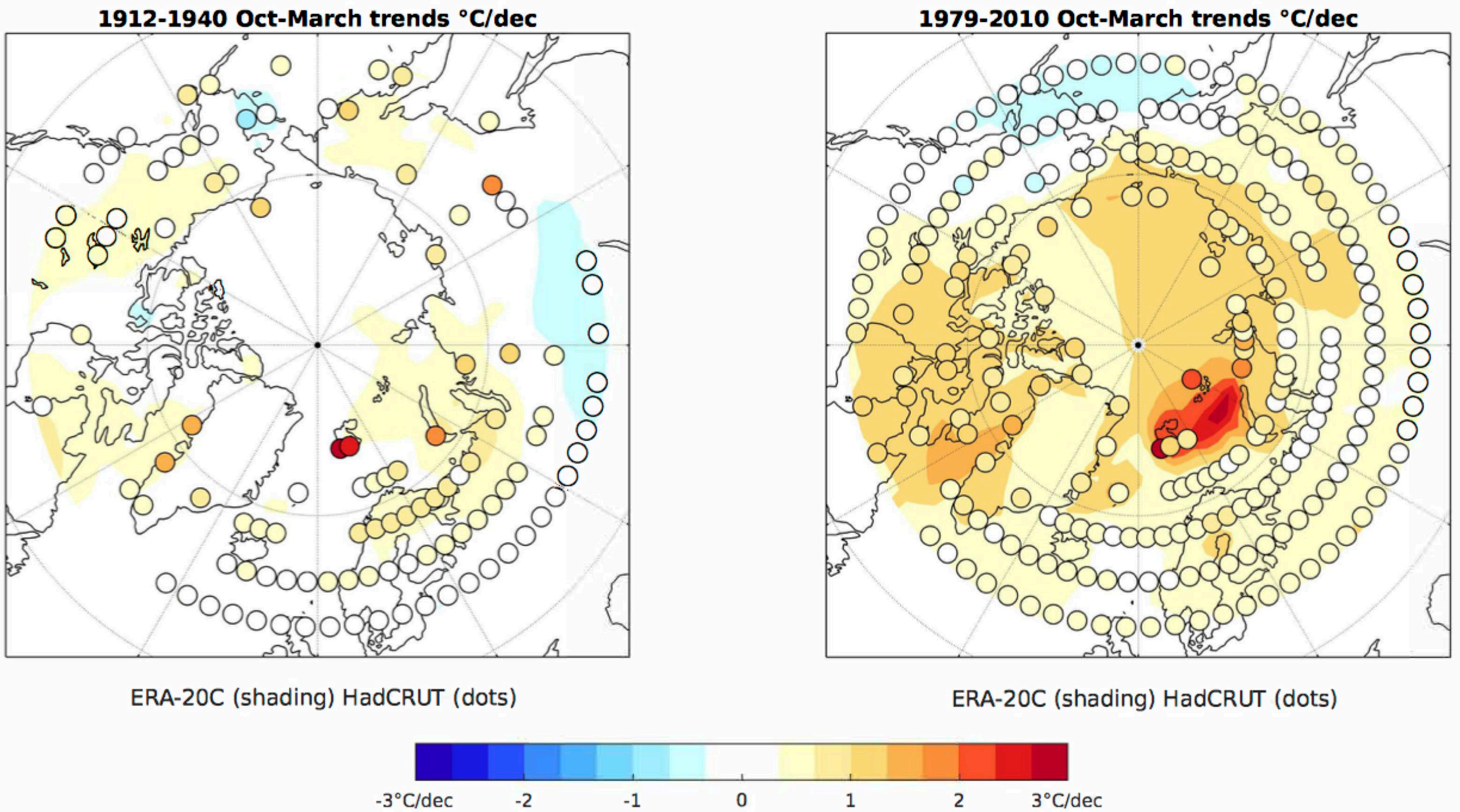
1912-1940 Oct-March trends °C/dec
1979-2010 Oct-March trends °C/dec
ERA-20C (shading) HadCRUT (dots)
ERA-20C (shading) HadCRUT (dots)
-3°C/dec
-2
-1
0
1
2
3°C/dec

Figure 3.

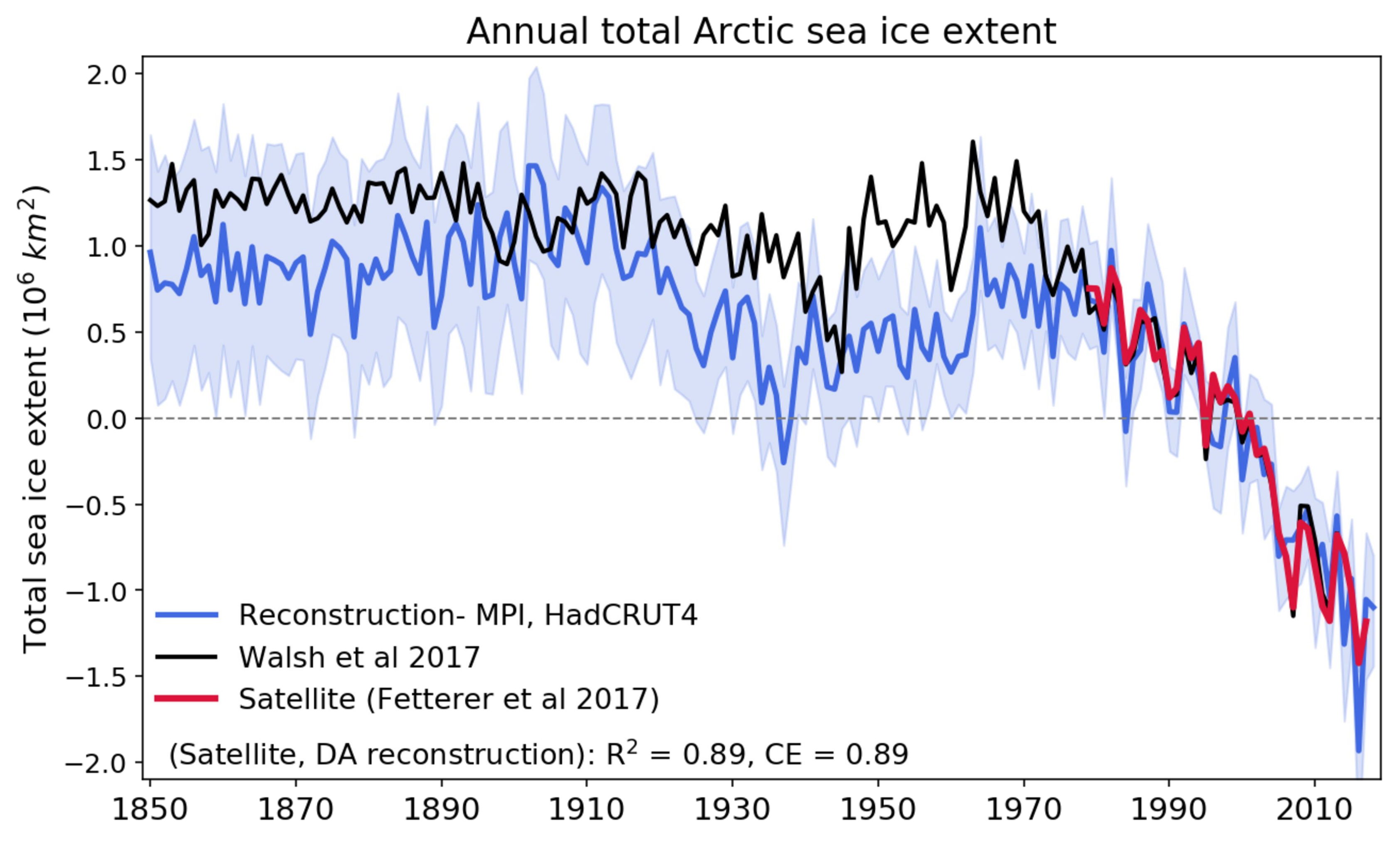

Annual total Arctic sea ice extent
Total sea ice extent (10^6 km^2)
2.0
1.5
1.0
0.5
0.0
−0.5
−1.0
−1.5
−2.0
1850
1870
1890
1910
1930
1950
1970
1990
2010
Reconstruction- MPI, HadCRUT4
Walsh et al 2017
Satellite (Fetterer et al 2017)
(Satellite, DA reconstruction): R^2 = 0.89, CE = 0.89

Figure 4.

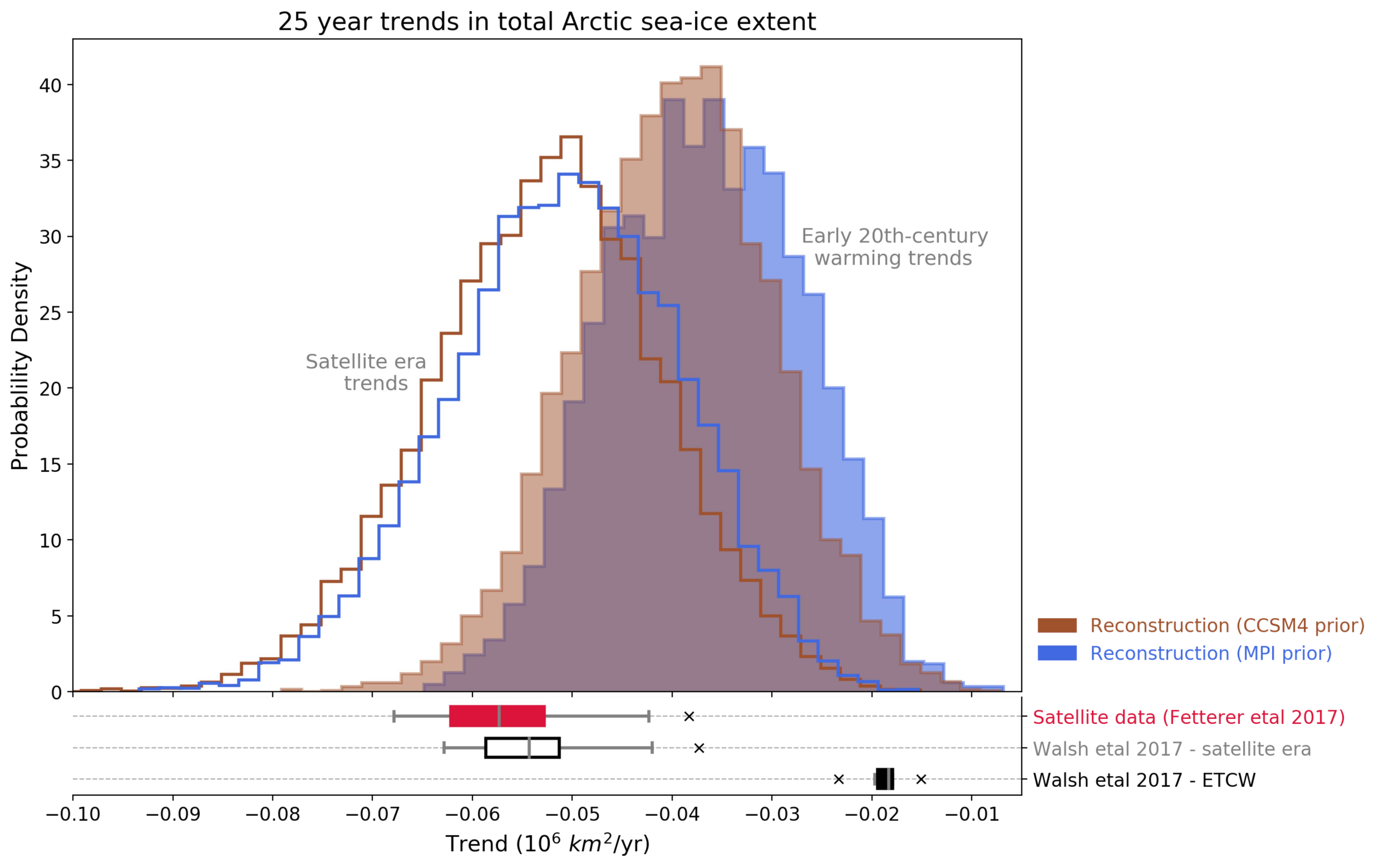
25 year trends in total Arctic sea-ice extent
Probability Density
Satellite era
trends
Early 20th-century
warming trends
Reconstruction (CCSM4 prior)
Reconstruction (MPI prior)
Satellite data (Fetterer etal 2017)
Walsh etal 2017 - satellite era
Walsh etal 2017 - ETCW
Trend (10^6 km^2/yr)
0
5
10
15
20
25
30
35
40
−0.10
−0.09
−0.08
−0.07
−0.06
−0.05
−0.04
−0.03
−0.02
−0.01

Supporting Information for “Arctic sea ice variability during the Instrumental Era”

M. Kathleen Brennan [1], Gregory J. Hakim[1], and Edward Blanchard-Wrigglesworth[1],

[1]Department of Atmospheric Sciences, University of Washington

Contents of this file

1. Data availability in Walsh et al 2017

Walsh et al. (2017) uses sea ice observations from a ranked list of 12 different sources. When none of these observation types are available at a given time, temporal interpolation (for a single month of missing data) or analog based methods to fill in missing data (for periods with more than one month missing) are used. In Figure S1 we plot the percentage

---

Corresponding author: M. Kathleen Brennan, Department of Atmospheric Sciences, University of Washington, Seattle, WA, USA (mkb22@uw.edu)

of longitude ocean grid cells with an observation available for each month separated into two seasons from 1850–2013. The vertical green lines indicate April and September of 1953 respectively. Before March of 1953 there is very little spatial coverage of sea ice observations in the winter months (September–March). Data coverage in the summer months (April–August) is also very low (<40% on average) before May of 1901 and then returns to full coverage intermittently between 1902–1953.

2. The early 20th century warming in reanalysis

Figure S2 shows a comparison between annually averaged Arctic (north of 70N) mean temperature observations from HadCRUT and reanalysis data (NOAA-20C and ERA-20C) during the 20th century. Between 1953–2011 there is good agreement between HadCRUT and ERA-20C with an R^2-value of 0.85 and R^2-value of 0.41 between HadCRUT and NOAA-20C. In contrast before, 1953 these two records diverge with an R^2-value of 0.27 and 0.01 respectively. Particularly from 1900–1953, ERA-20C temperature anomalies hover just below 0°C and NOAA-20C shows very cold anomalous temperatures of around -3°C, while HadCRUT increases from approximately -2°C to 1°C over the same time period. These discrepancies illustrate that neither of these reanalysis products capture the early 20th century warming.

3. Sensitivity of data assimilation results

Here, we quantify the sensitivity of our reconstructions to the choice of gridded temperature product assimilated (and their errors), climate model prior, and sample-error mediation in the DA (localization length scale and ensemble variance inflation factor).

3.1. Sensitivity to the observations

To test the sensitivity to the choice of assimilated observations, we assimilate three temperature products: HadCRUT, GISTEMP and Berkeley Earth (BE). The original temperature measurements used to create these products are mostly the same, and the main difference is the amount of interpolation (or infill) from grid cells with observations to grid cells with no observations for GISTEMP and BE. Reconstructions using all three temperature products are shown in Figure S3. The skill of the reconstruction during the satellite period is slightly higher when HadCRUT is assimilated, as measured by the R^2 values and coefficient of efficiency. Overall the source of the temperature observations has little effect on the overall variability of the reconstructions, with R^2 values with satellite data ranging from 0.82–0.89 for the MPI prior and 0.79–0.89 for the CCSM4 prior (described below). This is expected given the overall agreement among temperature products (e.g. (Rohde et al., 2013)).

For all of these experiments, an observed uncertainty of ($\mathbf{R}$ in Equation 2) 0.4 K^2 is used for all three products as explained in the main manuscript. Other uncertainty estimates tested include: (1) using the annually averaged diagonal elements of the error covariance matrix provided with HadCRUT, and (2) using the variance across all three datasets at each point. Method (1) is ideal, but can only be applied to HadCRUT which has fewer data points than GISTEMP and BE because it does not use interpolation. For method (2) the variance across these datasets is very small, given that they often use the same original temperature observations. This led to an over-weighting of observations in the

Kalman gain and a SIE reconstruction with an inter-annual variability much larger than the satellite record.

3.2. Sensitivity to the prior

We use the MPI and CCSM4 Last Millennium simulations to test the sensitivity of the results to the choice of model prior. Figure S3 shows Arctic SIE from these two experiments (note that we use different inflation factors of 1.8 and 2.6 for the MPI and CCSM4 priors respectively, see below). Results show differences in inter-annual variability, but overall the decadal variability and the timing and magnitude of the ETCW are in close agreement (Figure S3). MPI-based reconstructions show slightly higher correlation with satellite data, with R^2=0.82–0.89, as compared to CCSM4-based reconstruction, with R^2=0.79–0.89.

3.3. Sensitivity to sample error: prior inflation and localization

The prior ensemble-perturbation inflation factor and prior spatial localization length scale are both determined empirically based on correlations with the trend in Arctic SIE in satellite observations, and correlation and coefficient of efficiency with satellite observations between 1979–2017. A series of experiments are performed with inflation factors ranging from 1.6–2.0 (incremented by 0.1) for the MPI prior and 2.3–2.7 (incremented by 0.1) for the CCSM4 prior. For each inflation factor, reconstructions are performed for localization radii of 5,000, 7,500, 10,000, 15,000, 20,000, and 25,000 km. As the basis of comparison, the trend, detrended variance, correlation and coefficient of efficiency with respect to satellite observations between 1979–2017 are determined across all iterations and ensemble members for each of the 30 parameter combinations (see Figure S4 and S5).

Increasing the localization length scale and the ensemble inflation of sea ice relative to temperature, both increase the temporal variance and trend in the reconstructions of SIE (Figures S4, S5). The results indicate that there is not only a trade-off between capturing the trend versus the inter-annual variability, but that there are various parameter combinations that show similar performance. Overall, all experiments described above using HadCRUT observations resulted in R^2 values greater than 0.86 and CE greater than 0.77 for MPI and R^2 values greater than 0.76 and CE greater than 0.62 for CCSM4.

4. Verification Statistics

To test the performance of our reconstructions we use both R^2 value (correlation coefficient squared) and coefficient of efficiency against satellite observations. The coefficient of efficiency (CE), like the correlation coefficient, measures the synchronicity in the variability of two datasets, but also quantifies mean bias and the difference in variance between the two datasets. This is a much stricter skill metric. Its maximum value is 1.0 and it is unbounded in the negative direction. A CE value of zero occurs when the sum of squared errors is equal to the variance in the verification data. Generally, positive CE values represent skill. It is defined as:

$$CE = 1 - \frac{\sum_i^n (v_i - x_i)^2}{\sum_i^n (v_i - \bar{v})^2}. \tag{1}$$

Here v is the verification value and x is the value being evaluated (the reconstructed value).

References

Fetterer, F., Knowles, K., Meier, W. N., Savoie, M., & Windnagel, A. K. (2017). Sea Ice Index, Version 3. *NSIDC: National Snow and Ice Data Center, Boulder, Colorado USA*. doi: 10.7265/N5K072F8

Rohde, R., Muller, R., Jacobsen, R., Perlmutter, S., & Mosher, S. (2013). Berkeley Earth Temperature Averaging Process. *Geoinformatics & Geostatistics: An Overview*, *01*(02). doi: 10.4172/2327-4581.1000103

Walsh, J. E., Fetterer, F., Scott Stewart, J., & Chapman, W. L. (2017, jan). A database for depicting Arctic sea ice variations back to 1850. *Geographical Review*, *107*(1), 89–107. doi: 10.1111/j.1931-0846.2016.12195.x

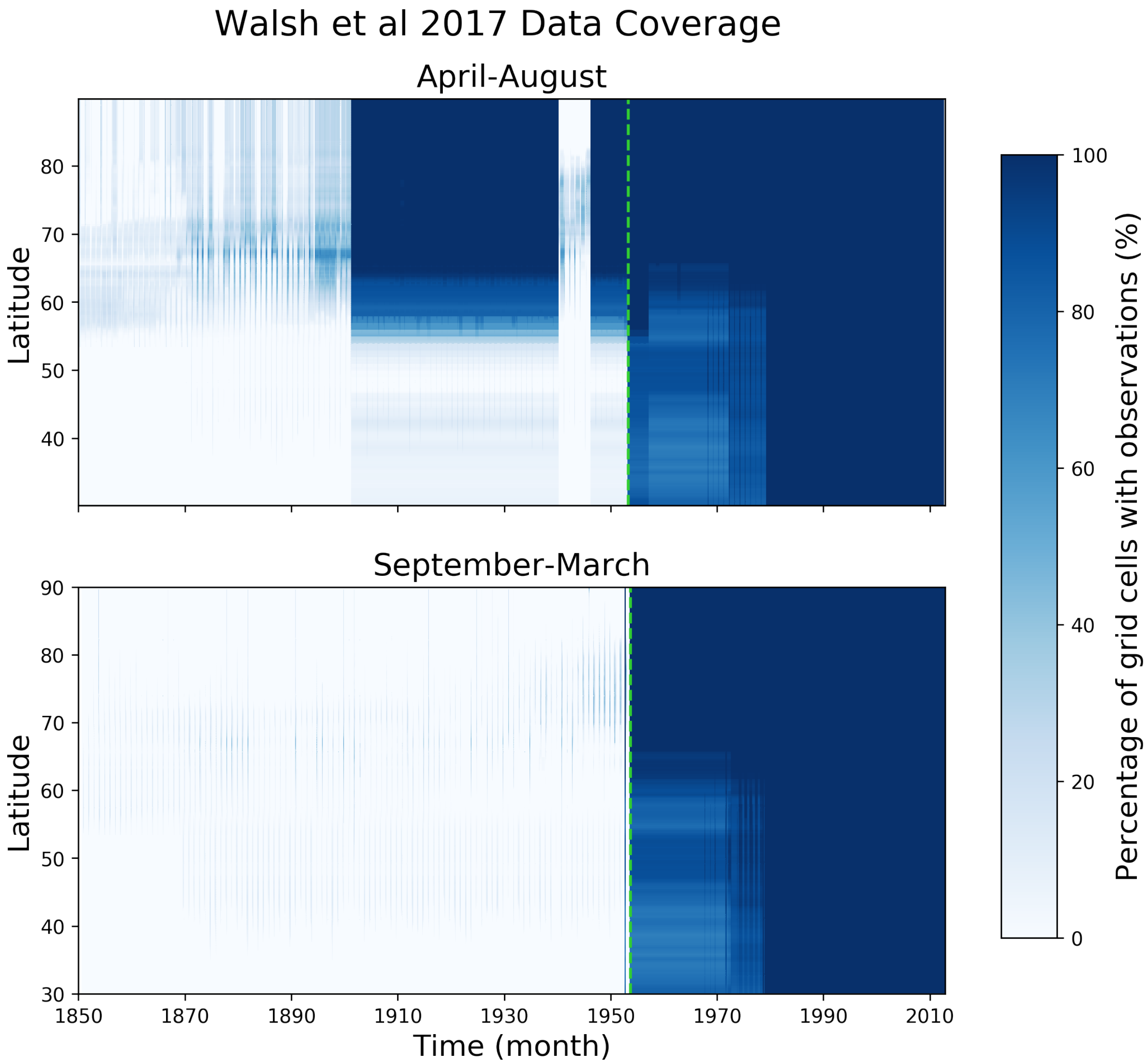

Figure S1. Shown is the data availability incorporated into the Walsh et al. (2017) Arctic sea ice record separated by two seasons over time. The color indicates the percentage of ocean longitude grid cells with an observation available at each latitude for each month. The vertical green lines indicate April 1953 and September 1953 respectively.

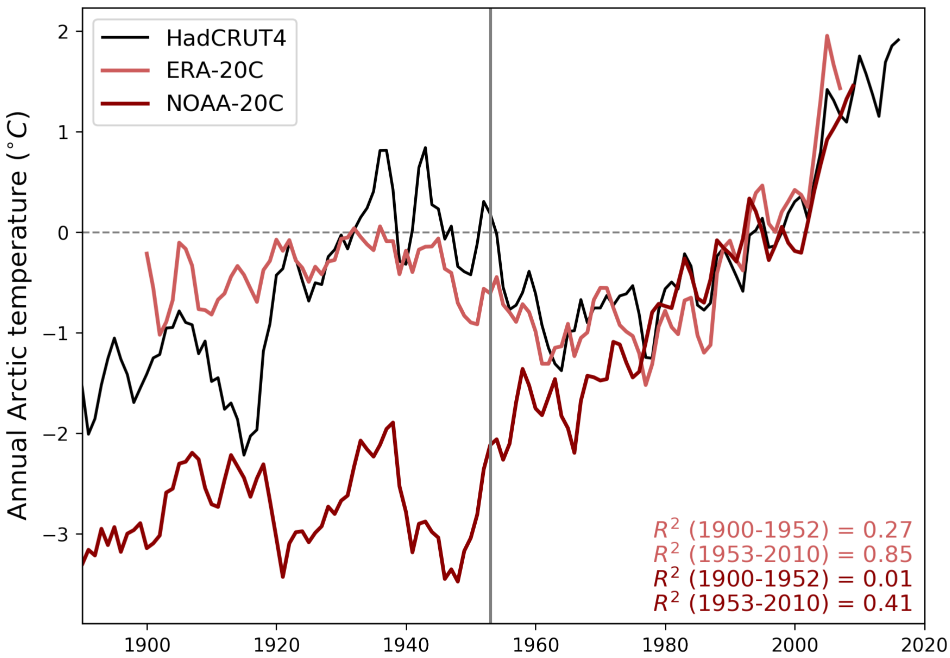

Figure S2. Arctic (north of 70N) mean surface air temperatures anomalies from HadCRUT, NOAA-20C, and ERA-20C. The vertical gray line indicates the year 1953, when availability of observations of sea ice in the Arctic decline substantially in the Walsh et al. (2017) record. Anomalies are centered about 1979-2011.

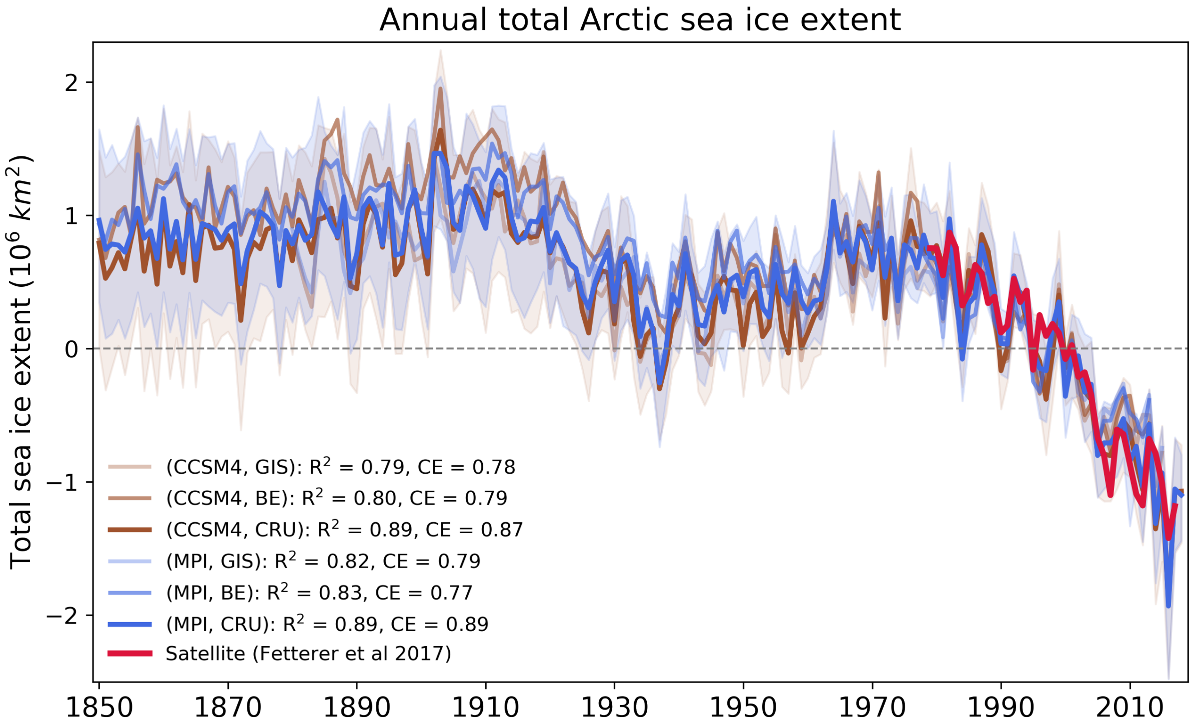

Figure S3. Total Arctic SIE reconstructed using priors drawn from two models (MPI and CCSM4 Last Millennium simulations) and three temperature datasets (HadCRUT, GISTEMP, and BE). For all experiments a localization length scale of 15,000 km is used and an inflation factor of 1.8 for MPI and 2.6 for CCSM4. The 97.5 and 2.5 percentiles of the ensemble spread are shown in blue and brown shading.

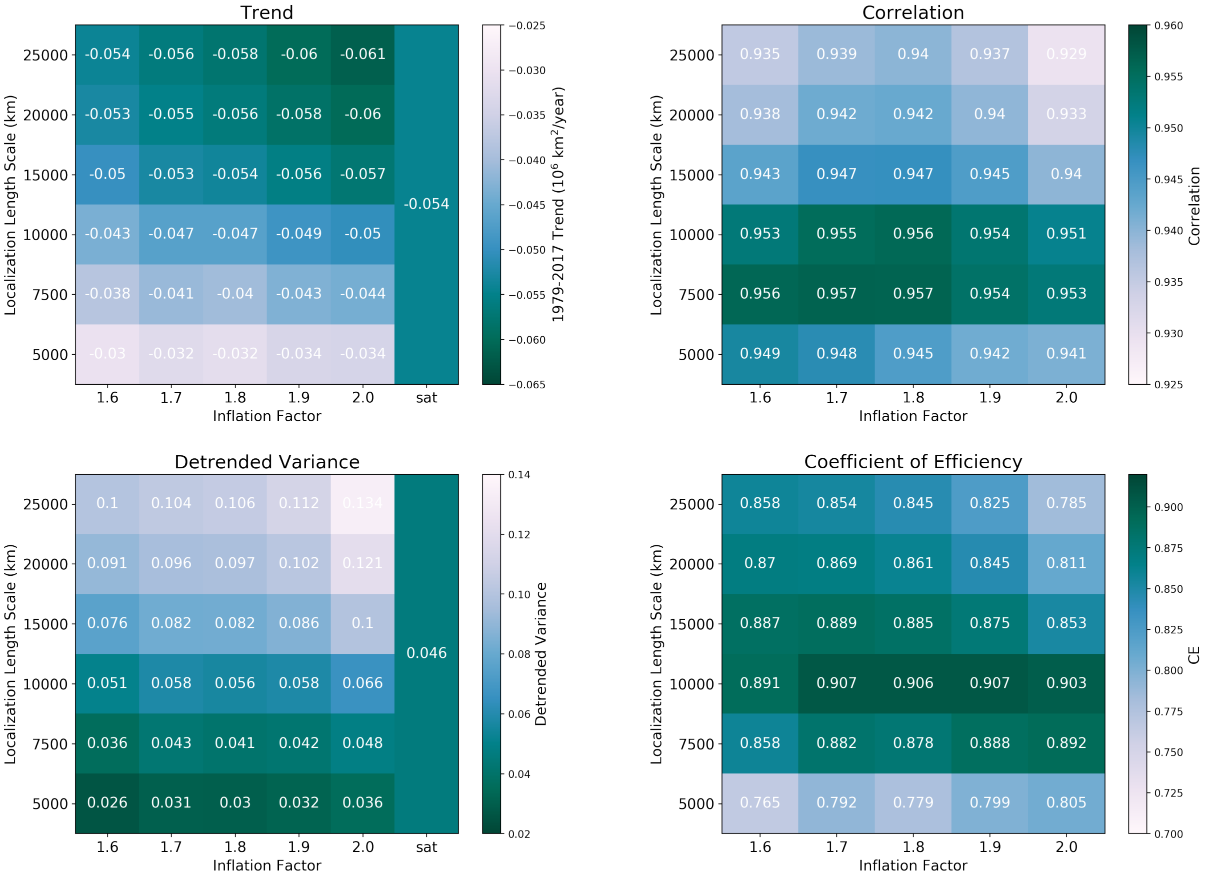

Figure S4. Verification statistics for 30 reconstructions performed using MPI as a model prior, HadCRUT observations, and different combinations of localization length scales (y-axis) and inflation factors (x-axis) are shown. Trends and detrended variances during the satellite era are shown in the two boxes on the left and the values observed in the satellite record (Fetterer et al., 2017) are shown in the column on the right. The correlation and coefficient of efficiency of these reconstructions when compared with (Fetterer et al., 2017) are shown in the two boxes on the right.

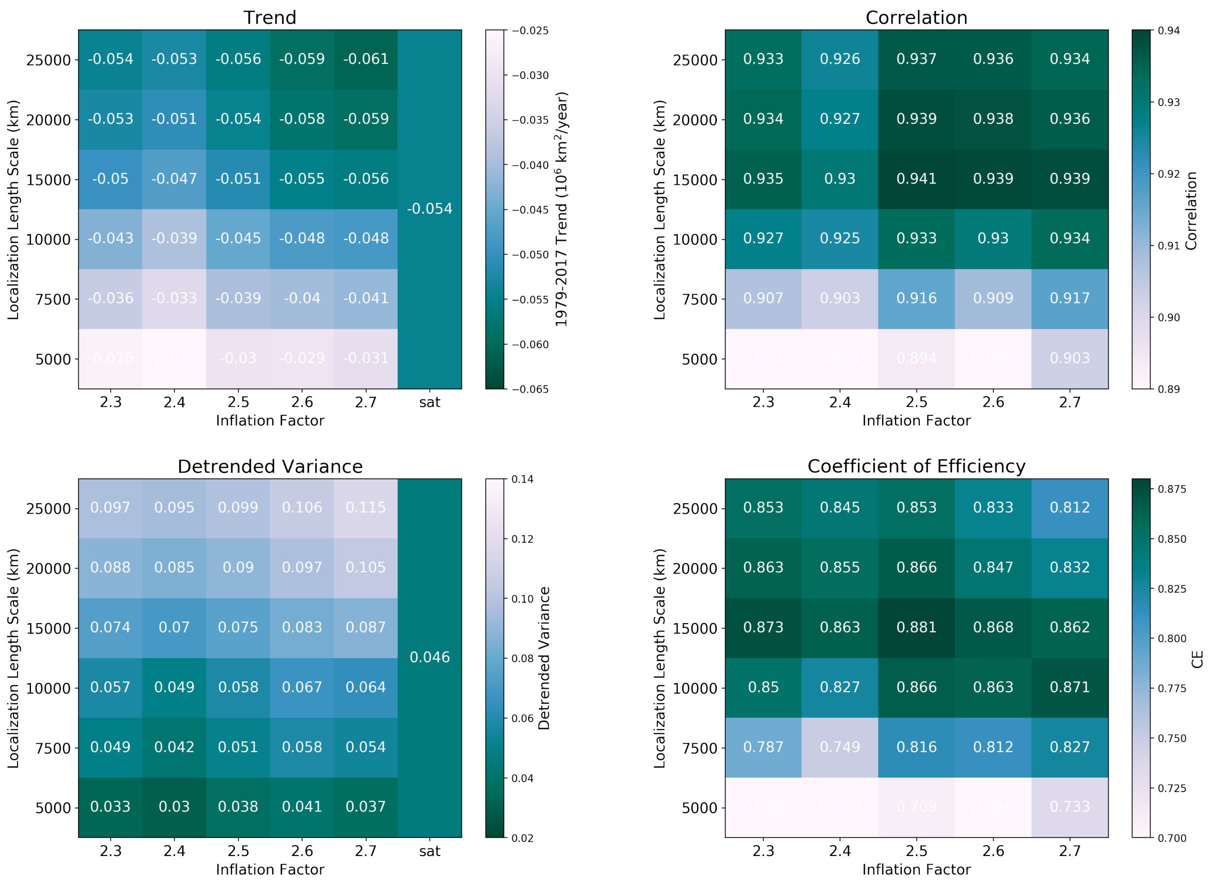

Figure S5. Verification statistics for 30 reconstructions performed using CCSM4 as a model prior, HadCRUT observations, and different combinations of localization length scales (y-axis) and inflation factors (x-axis) are shown. Trends and detrended variances during the satellite era are shown in the two boxes on the left and the values observed in the satellite record (Fetterer et al., 2017) are shown in the column on the right. The correlation and coefficient of efficiency of these reconstructions when compared with (Fetterer et al., 2017) are shown in the two boxes on the right.